Published in final edited form as:
Exp Cell Res. 2010 January 1; 316(1): 103–114. doi:10.1016/j.yexcr.2009.08.005.

Experimental control of excitable embryonic tissues: three stimuli induce rapid epithelial contraction

Sagar D. Joshi[*], **Michelangelo von Dassow**[*], and **Lance. A. Davidson**[1]
Department of Bioengineering, University of Pittsburgh, 3501 Fifth Ave., Pittsburgh PA, 15260

Abstract

Cell generated contractility is a major driver of morphogenesis during processes such as epithelial bending and epithelial-to-mesenchymal transitions. Previous studies of contraction in embryos have relied on developmentally programmed cell shape changes such as those that accompany ventral furrow formation in *Drosophila*, bottle cell formation in *Xenopus*, ingression in amniote embryos, and neurulation in vertebrate embryos. We have identified three methods to reproducibly and acutely induce contraction in embryonic epithelial sheets: laser activation, electrical stimulation, and nano-perfusion with chemicals released by wounding. Contractions induced by all three methods occur over a similar time scale (1 to 2 min) and lead to reorganization of the F-actin cytoskeleton. By combining induced contractions with micro-aspiration we can simultaneously measure the stiffness of the tissue and the force and work done by contractions. Laser-activation allows real-time visualization of F-actin remodeling during contraction. Perfusion with cell-lysate suggests these three stimuli activate physiologically relevant pathways that maintain epithelial tension or trigger epithelial morphogenesis. Our methods provide the means to control and study cellular contractility and will allow dissection of molecular mechanisms and biomechanics of cellular contractility.

Keywords

developmental biomechanics; stimulated contraction; morphogenesis; F-actin; epithelia; apical contraction

Introduction

Cell contraction is a major contributor to the forces that shape tissues during morphogenesis and organogenesis in multicellular organisms. As groups of cells contract in epithelia they can narrow their apices to form wedge or bottle-shaped cells. Coordinated contraction has been proposed to drive a wide variety of morphogenetic events such as sea-urchin gastrulation [1], *Drosophila* ventral-furrow formation [2], and neurulation in vertebrates [3,4]. Furthermore, cell contraction in single epithelial cells occurs during epithelial-to-mesenchymal transitions in gastrulating amniotes [5], dorsal closure in *Drosophila* [6], and wound healing in *Xenopus laevis* [7]. These developmentally programmed events form the basis of our understanding of the role of contraction and provide clues to the molecular mechanisms.

[1]corresponding author; lad43@pitt.edu; phone: 412-383-5820.
[*]equal contributions

Pulsed contractions of actomyosin within the apical cortex are thought to drive morphogenetic movements of ventral furrow formation [8,9], as well as closure of the amnioserosa in *Drosophila* [6]. Pulsed contractions typically occur within the actin-rich apical cortex, however, actomyosin dynamics within the circum-apical belt, along baso-lateral membranes, as well as microtubule dynamics along the apical basal axis of epithelial cells are all believed to play a role in generating forces of cell shape change within epithelial cells.

The capacity to acutely control and manipulate cellular contractility in the embryo would provide novel approaches for investigating pathways that control contractility, and would aid in disentangling active from passive mechanical properties of embryonic cells [10]. In this paper we first demonstrate three experimental methods to induce contractions in amphibian embryos. Using perfusion of cell lysate, electrical stimulation, and laser-activation we induce contractions within 10 to 20 seconds. While these three methods involve different activation pathways we propose they utilize the same downstream biochemical pathway culminating in rapid F-actin remodeling, and contraction of the apical surface of stimulated epithelial cells. We then use these three different stimuli to investigate relationships between stiffness and force generation in embryonic tissues. These approaches will provide new tools for investigating cell and tissue mechanics in embryos.

Methods

Embryo handling, microsurgery and culture media

Eggs from female *Xenopus laevis* frogs were collected and fertilized following standard methods [11] and were dejellied in 2% Cysteine solution (pH 8.4) 20 minutes after fertilization. Embryos were cultured in 1/3x Modified Barth's solution (MBS) to late blastula or early gastrula stages [12] and vitelline membranes were removed using forceps. Since exposure to lysed embryos can cause epithelial contraction care was taken to minimize wounding of embryos for the whole embryo experiments. For laser activation experiments, animal cap explants were microsurgically removed from stage 10.5 embryos using custom-made hair-loops and hair–knives in Danilchik's For Amy (DFA; [13]). With care, microsurgery with hair-tools results in minimal cell lysis. Unless otherwise mentioned, whole embryos at early gastrula stage were cultured in 1/3x MBS and explants harvested from early gastrula stage embryos were cultured in DFA. Bovine serum albumin (0.1 or 0.2 % in media; Sigma-Aldrich, St. Louis MO) and antibiotic/antimycotic (0.8 % in media; A5955, Sigma-Aldrich) were added to both 1/3x MBS and DFA. Unless otherwise stated, experiments were done at early- to mid-gastrulation (stages 10 to 11).

Microscopy

Nano-perfusion experiments were recorded by a digital charge-coupled device (CCD) camera (Scion Corp., Frederick, MD) mounted on a dissecting stereoscope. To visualize embryos and explants during nano-perfusion time-lapse sequences were collected at 1 to 2 second intervals using computer controlled acquisition software (ImageJ, Wayne Rasband NIH). Electrically stimulated embryos held within the micro-aspirator were visualized using an inverted compound microscope (Leica Microsystems, Bannockburn IL) with either a CCD camera (Scion Corp) or a confocal scan head (Leica TCS SP5). Laser activation experiments were recorded using a confocal scan head mounted on an inverted compound microscope. Time-lapse sequences from all three experiments were analyzed either manually or with custom-image processing macros (ImageJ).

Fluorescent probes, Lineage Labels, and Fluorescent proteins

Embryos at the 1- to 4-cell stage were briefly cultured in 3% Ficoll (Sigma, St. Louis MO) in 1x MBS and microinjected with desired volume of capped mRNA encoding GFP targeted to

membrane (mem-GFP) or F-actin (moe-GFP). Capped mRNA was synthesized and purified by standard methods from linearized DNA template (AmpliCap Transcription kit; Epicentre Biotechnologies, Madison WI).

Apparatus and analysis for three methods to induce contraction

(1) Micro-aspiration and electrically stimulated contraction—We first describe our updated micro-aspiration device and then its modification for simultaneous measurement of physical mechanical properties during aspiration and force production during electrical stimulation. Our micro-aspirator consists of two 90 × 90 mm chambers, a high-pressure and a low-pressure reservoir, connected by a piece of poly(dimethylsiloxane) (PDMS) cast around a glass fiber to leave a 120–125 μm diameter channel connecting the two reservoirs (figure 1A; described in detail in [14]). Whole embryos (~1400 μm diameter) are gently pressed to the channel opening on the high-pressure reservoir side, and suction is applied to the embryo at the desired tissue location. The pressure difference between the reservoirs is controlled hydrostatically by adjusting the water level in the low-pressure reservoir. An updated design allows us to adjust the water level either manually with a syringe or using a computer controlled linear actuator (NA08A30A, Zaber Technologies) that drives a piston. Both the camera and the linear actuator are controlled by image acquisition and hardware automation software using a custom macro (LabView VI; National Instruments, Austin TX). Using the linear actuator, we are able to change the pressure across the micro-channel at a user defined speed, e.g. drop pressure 5.4 Pa linearly over 2 seconds. Our micro-aspirator design allows extremely fine control of the pressure at the desired range (≤10 Pa) and clear views of the aspirated tissue [14]. Loading suction pressures were −5.4 Pa above a pre-load baseline pressure of −1.2 Pa.

We calculate an apparent stiffness [14] of the patch of tissue in the micro-channel from the applied pressure and the time dependent aspirated length using linearly elastic models of micro-aspiration [15,16]. Over the range of pressures used, embryonic tissue behaves linearly with pressure as expected for these models [14]. We performed micro-aspiration on the dorsal marginal zone where tissues were thick enough relative to the channel diameter to approximate with a half-space model (infinite tissue thickness; [14]) in all experiments except those involving the confocal. Precise positioning was difficult with the confocal mounted micro-aspirator, so stiffness measurements were not made.

The PDMS channel of our micro-aspirator allows electrical stimulation of aspirated tissue at the same time as measuring its mechanical properties. Electrical current was provided by threading a Platinum-Iridium electrode (A-M Systems, Sequim, WA) through the channel to within 3 to 4 mm of the embryo, and placing a large Platinum-Iridium counter electrode in the high-pressure reservoir. Single electrical pulses with duration of ~80μs and a mean voltage of ~10 V were generated using a stimulus isolator (WPI A320; World Precision Instruments, Sarasota FL). Unless otherwise stated, the channel was negative with respect to the embryo (“outward current”).

To visualize actin dynamics within micro-aspirated tissues we built a smaller version of the micro-aspirator for use with a confocal microscope. The same PDMS channels are used, but the high- and low-pressure reservoirs were 21.4 × 33.3 mm wide, and a glass cover-slip below the micro-channel to served as a window. Pressure was adjusted by removing media from the low-pressure reservoir with a manual pipette. Embryos were held to the micro-channel opening with a wedge shaped well in a PDMS block and by lightly compressing the embryo with a small glass coverslip fragment.

Briefly, the protocol for measurement of contraction following electrical stimulation begins with a standard stiffness measurement (see above). At a pre-determined time after the start of micro-aspiration an electrical pulse, or pulse-train, is delivered across the micro-channel. A

visual recording of the time-course of the micro-aspiration and electrical stimulation is collected and subsequently analyzed to estimate both the mechanical properties and strength of the electrically-stimulated mechanical response.

(2) Laser activated contraction—We integrated a manual laser ablation system (Micropoint, Photonic Instruments Inc, St. Charles, IL) with the confocal microscope so that we could laser-activate precise locations and collect confocal time-lapse sequences before and immediately following laser activation (figure 1D). The integrated system consists of a fiber optically delivered beam from a nitrogen-pumped dye laser, beam steering optics and interference filters allowing precise cell membrane ablations or cell targeting. Spatial alignment and focusing of the target illumination is manually controlled. A manually driven optical attenuator allows us to adjust the power of the laser pulse and the size of spot stimulus.

In brief, the protocol for laser activation begins with the preparation of an animal cap explant from the animal pole of a gastrulating embryo (between stages 10 and 10.5). Explants and embryos were gently compressed under a glass coverslip bridge held in place with high vacuum silicone grease (Dow Chemical, Russellville, AR) in a custom glass-bottomed confocal chamber. The glass coverslip and confocal chamber were pre-treated with 1% bovine serum albumin (BSA) to avoid sticking or wounding of the embryo. The chamber was then sealed for long-term stable confocal imaging and placed on the stage of the microscope. A suitable field of cells was selected and a pre-activation time-lapse sequence was collected. A predetermined cell or cell-cell junction was targeted with and ablated with 1 to 5 laser pulses. Similar number of pulses were used within an experiment. The number of pulses changed in different experiments depending upon the cell pigmentation that could vary between different clutches of embryos. A second time-lapse sequence was immediately started and collected for 3 to 20 minutes.

(3) Nano-perfusion stimulated contraction—After initial studies identified a role for cell-lysate in inducing embryonic tissue contraction (LD and R. Hillenbrand, personal observations) we adopted a simple yet precise approach for delivering user specified quantities of lysate over a defined time-course. We first prepared cell lysate by tritrating two early gastrula embryos in 100 μl 1/3x MBS. Lysate was mixed and centrifuged at 13000 rpm allowing separation of large organelles from supernatant subsequently used for perfusion. 100 μl of the lysate was mixed with 3μl black non-waterproof ink (Higgins Fountain Pen India Ink; Utrecht Art, Cranbury NJ) to allow us to see the applied lysate. To deliver precise amounts of lysate we used a nano-injection apparatus (PLI-90; Harvard Apparatus, Holliston MA), loaded lysate into glass micro-needles, and adjusted the injection time and pressure to deliver 60 nl in a single pulse. Delivery of lysate and the mechanical response of the embryonic tissue was recorded (figure 1H).

Briefly, the protocol for stimulating contraction via nano-perfusion begins with the selection of gastrula stage embryos and removal of the vitelline membrane. Whole embryos are transferred into fresh media and visualized with a CCD equipped stereoscope. The target tissue and micro-needle are aligned so that the epithelial surface is in focus and opening of the needle is visible within the image field. Since contact between the micro-needle and the embryo could wound the embryo, care is taken to ensure that the micro-needle does not touch the embryo. A time-lapse collection is started and a bolus of lysate is injected over the tissue surface by manually triggering the nano-injection apparatus. Bulk tissue movements of the contraction response were analyzed with kymographs prepared from the time-lapse sequences (ImageJ).

Results

Three stimuli produce contractions with similar kinematics

Electrical stimulation (figure 1A, B, and C, supplemental video S1), laser activation (figure 1D through G, supplemental video S2), and nano-perfused lysate (figure 1H, I, and J, supplemental video S3) all induce rapid contractions of the epithelial tissue beginning 10 to 20 seconds, and continuing for the subsequent 30 to 90 seconds after stimulation. After an electrical pulse is delivered to a micro-aspirated embryonic tissue the tissue contracts and can partially withdraw from the micro-channel (figure 1B and C). Withdrawal consistently begins within 10 to 15 seconds reaching a peak contraction at 45 to 90 s, and then slowly relaxes towards the original tissue position (figures 1C and 2A-B). After a laser pulse is delivered to a central cell or cell-cell membrane the surrounding cells, out to the edge of the field of view (figure 1E; more than 10-cell diameters), begin to contract within 10 to 20 seconds (figures 1F and 2C-D). Cell contractions appeared isometric. Contraction is rapid over 60 seconds and then slows (figures 1G and 2D). Since the laser activation damages single or multiple cells (contraction does not require ablation), long time-scale wound healing response begins about 3 minutes after activation and culminates in the removal or excision of the damaged tissue (data not shown). Nano-perfusion of a bolus of 60 nl of cell lysate stimulates contraction of cells in direct contact with the lysate within 10 to 20 seconds (figures 1J and 2E-H). Contractions were not stimulated by nano-perfusion with ink-labeled 1/3x MBS (n = 6). Lysate-induced contraction continues and reaches a peak within 30 to 60 seconds and then slowly relaxes. Hence, all three methods for stimulating contraction produce kinematically similar results. Laser-activation contrasts with the other methods in that the contraction-response is prolonged, however, the initial rapid contraction is similar among all three methods (figure 2). Wound healing following laser activation could account for the differences in kinematics after the initial phase of contraction.

Consistent with previous observations [14], we found no evidence that mechanical stimulation induces contractions. Contractions following pressure changes were very rare, and the great majority of embryos tested behaved as expected for a passive viscoelastic material exhibiting power-law creep compliance (supplemental figure S1). Furthermore, embryos which were poked with a micro-needle but not wounded did not exhibit contractions (n = 7), in contrast, poked embryos in which a single cell was wounded did exhibit contractions (n = 8; supplemental video S4).

For technical reasons (see “Methods”) our quantitative studies focused on the DMZ for electrically stimulated contractions, and the animal cap for laser and lysate induced contractions, qualitatively similar contractions were observed in most other regions of the embryonic epithelium. Electrical stimulation induced contractions at all tested locations (DMZ, ventral side, animal cap, and vegetal endoderm); lysate induced contractions occurred in most tested regions of the epithelium, with the sole exception of the endoderm; and laser activation induced contractions in the two tested regions: animal cap and DMZ. Albino embryos did not contract in response to laser stimulation (n = 4), suggesting that pigment granules are required for laser activation of contractions, possibly due to their high optical absorbance. In addition, while we focus on early to mid gastrulation stages (st. 10 to st. 11), lysate and laser induced contractions were observed at all tested stages (stages 10 to 16). Electrical stimulation was only tested at stages 10 to 11.

All the stimulation techniques and methods used to observe contraction are different but we can compare and contrast several features of the responding tissues including: 1) changes in the mechanics and architecture of the tissue, and 2) responses to multiple stimuli. Stimulated tissues respond quickly to activation and the response persists for one to several minutes (figure 2A, C, and E). In all cases the initial response to stimulation is delayed by ~10 to 20 seconds

(figure 2B, D′, F, and G), and the response increases over the next 40 to 60 seconds. Contractions after single electrical or nano-perfusion stimulation are often completely reversible producing little permanent change to the tissue. Long-lasting contractions after laser activation "over-shoot" the response needed to remove or replace tissue damaged by laser (dotted lines in figure 2D). In contrast, electrical stimulation does not appear to alter the mechanical properties of the micro-aspirated tissue (figure 2A and Table 1; "creep" is 7 ± 7 μm [mean ± SD] in unstimulated vs. 5 ± 6 μm in stimulated tissues; "relaxation" is 6 ± 2 μm in unstimulated vs. 6 ± 4 μm in stimulated tissues). Electrically stimulated embryos were close in stage (st. 10 to st. 10.5), so stage-to-stage variation would contribute little to the observed mechanical variation. The few embryos that displayed contractions independently of electrical stimulation did not affect these results.

Another characteristic shared by these methods is their response to multiple stimuli. In the course of evaluating the response to differing current polarities micro-aspirated tissues could be stimulated up to 4 times (figure 3A) with no detectable differences in the magnitude or timing (figure 3B) between first and second stimulus at a given polarity ($P \geq 0.6$ for both comparisons; n = 10; outward current; Wilcoxon signed ranks test). Here, four stimuli were given to each embryo, 7 minutes apart, with two stimuli at each polarity. The order of stimulus polarities was randomized for each embryo. The magnitude of electrically stimulated contractions depended strongly on the polarity of the applied current (figures 2B and 3B; $P = 0.002$; n=10; average of the two stimuli given to each embryo at a given polarity; Wilcoxon Signed Ranks test). Outward current passing from the embryo into the micro-aspiration channel generated nearly a 2-fold increase in the retraction distance. Multiple contractions induced by repeated laser activation (figure 3C through F) and nano-perfusion (figure 3G) are qualitatively similar to repeated contractions following electrical stimulation. Even though the physical means of stimulation are different, the contraction response of tissues subjected to electrical stimulation, laser activation, and nano-perfusion of cell lysate are remarkably similar in their timing and response to repeated stimulation.

Although technical constraints make it difficult to compare the spreading of contractions from the stimulated site among the methods of inducing contractions, there was some evidence that the amount of spreading differed. There was no correlation between the amount of cell contraction and the distance from the site of laser activation within the field of view (within ≤ 250 μm; supplemental figure S2). In contrast we did not observe contraction at positions that were distant from the site of lysate application. Laser activation required the use of high magnification oil immersion lenses, whereas lysate application required space to expose tissue to the lysate, limiting most experiments to low magnification stereoscope views. Furthermore, although ink-labeling the lysate allowed visualization of the media containing the lysate, it does not provide information on lysate concentrations. However these data suggest that laser-induced contractions spread quite far from the laser-activated cell, whereas lysate-induced contractions may not spread beyond directly stimulated cells.

Contraction is accompanied by rapid re-modeling of the F-actin cytoskeleton

Since the F-actin cytoskeleton plays an important role in cell contraction, the establishment of tissue mechanical properties, and mechanical events of morphogenesis in general we wanted to understand how the F-actin cytoskeleton was altered during the course of induced contraction. Cell and tissue contraction is thought to be driven by a number of different cellular mechanisms including: 1) whole cell contraction, 2) apical-basal contraction, 3) circum-apical or circum-basal contraction, and 4) apical cortex contraction. Each of these cellular mechanisms depend critically on remodeling of the F-actin cytoskeleton (for instance see [6, 8,17]).

In order to visualize F-actin dynamics during stimulation we expressed a fluorescently tagged fragment of the actin binding protein moesin (moe-GFP; [18]). Embryos injected with 0.5 to 1.0 ng of moe-GFP mRNA at the 1 cell-stage allowed observation of F-actin dynamics that were confirmed with a second actin-binding protein, utrophin-GFP [19]. Due to the geometric constraints of our three stimulation methods we focused on the remodeling of F-actin by laser-activation of the apical face of epithelial cells (figure 4A,supplemental video S5). Laser-activation of a single cell produced rapid F-actin accumulation throughout the field of view. The baseline intensity of F-actin within epithelial cells in the animal cap varies due to variable pigmentation in the animal cap. Raw intensity of F-actin within the apical cell cortex increases rapidly after a short 10 to 20 second delay and peaks within 60 seconds (figure 4B). Normalized F-actin intensity profiles highlight variable responses by individual cells after the initial peak (figure 4C; cell identities correspond to those in A and B). Some cells within the field return to pre-laser activation levels while most show a persistent 50% increase in intensity (20 cells in 4 explants; figure 4D). In some instances we observed actin “comets” consisting of moving spots of intense F-actin reminiscent of F-actin structures observed in cultured cells [20,21]. Visualization of F-actin in XZ-slices confirmed that increases in F-actin intensity following laser activation were the result of F-actin accumulation, rather than merely displacement of the F-actin cortex (supplemental figure S3).

We qualitatively confirmed similar patterns of F-actin dynamics during perfusion and electrical stimulation after adapting these protocols to use confocal imaging. Although visualization through the PDMS and the curved micro-channel was challenging, by reducing the size of our micro-aspirator to fit on the confocal (see methods) we could image the embryo’s epithelium and remained able to make out the apical cortex and circum-apical bands of F-actin (figure 4E). After electrical stimulation we were able to confirm increases in F-actin near the membrane and features such as actin comets and persistent spots reminiscent of F-actin remodeling after laser activation (figure 4F, supplemental video S6). We could see such features in most embryos following electrical stimulation but there was considerable variability. To confirm that we were observing changes in F-actin rather than simply cell-shape changes we electrically stimulated embryos expressing a plasma-membrane targeted GFP (figure 4G). The membrane label shows cell shape changes but does not show the same localized spots of increased intensity seen in the case of moe-GFP expressing embryos.

We modified our nano-perfusion stimulus to observe F-actin within animal cap explants (figure 4I through L). Explants were used here because large-scale movements in whole embryos prevented continuous visualization of F-actin. Lysate-induced contractions appear to be similar in both explants and whole embryos. The challenge to tracking F-actin in perfused tissues lies not with the optics but rather with the delivery of a high concentration of lysate to the tissue. Even so, we were able to confirm F-actin comet formation and F-actin intensity increases at the basal cell cortex (cells adherent to fibronectin; figure 4I and J) and recruitment of F-actin to the lateral cell cortex (figure 4K and L) after addition of lysate to the confocal chamber. Thus, the kinematics of cell shape change and tissue deformation, and the accumulation of F-actin appear similar after stimulation by laser-activation, electrical stimulation, and nano-perfusion.

Does tissue stiffness affect contraction strength?

Early morphogenesis is unexpectedly robust in the face of variation in tissue stiffness [14,22, 23]. One could explain this robustness to mechanical variation if a tissue’s capacity to produce force is proportional to its stiffness. Thus, force-production would need to increase in stiffer embryos or as the embryo ages. For instance, stiffer embryos would compensate for their increased resistance to deformation by producing more force. This hypothesis has some molecular basis as well since contractility and the initial stiffness of the epithelium may both

depend on the cytoskeleton. To test this hypothesis we compared mechanical properties with the forces and work produced by a contraction in the same tissue.

Two measures of the mechanical output of a contraction of the aspirated tissue are: 1) the work produced, and 2) the force per unit area (stress) required to generate the observed degree of contraction (figure 5A). Work can be measured in the micro-aspirator by measuring the change in aspirated volume due to the contraction multiplied by the total suction pressure acting on the tissue. Total suction pressure is the sum of the pre-load (P_0) and the load (ΔP) pressures. We approximate the volume change by the maximum change in aspirated length during the contraction (m; figure 2A) multiplied by the area of the channel. Hence, work per area (W) is:

$$W \approx (\Delta P + P_0) * m \quad (1)$$

The stress required to generate the observed contraction can be estimated as a pressure change required to induce the same level of contraction ("equivalent stress", S). Since the change in aspirated length following suction is approximately linear with pressure at the range of pressures used [14], the equivalent stress is calculated as the product of the load pressure and the displacement following contraction, divided by the change in aspirated length (D) following application of the load suction:

$$S \approx \Delta P^* m/D \quad (2)$$

We found no detectable relationship between the apparent stiffness of the tissue (measured at 300 s) and the contraction strength measured either as work or as equivalent stress (figure 5B; Table 2). Much of the variation may be due to clutch-to-clutch variation among *X. laevis* embryos [14]. All embryos were at stage 10 to 10.5, so stage-to-stage variation would not contribute substantially to the observed mechanical variation.

Discussion and Conclusion

We have investigated electrical stimulation, laser activation, and nano-perfusion methods for inducing acute cell contraction within embryonic epithelial cell sheets. Each of these three stimuli produce similar contractions in the targeted epithelium including a 10 to 20 second delay between stimulation and the start of contraction and rapid movements lasting about 60 seconds. However, there are differences in the responses. For instance, laser-activation appears to stimulate a long time-scale wound healing response causing "over-shoot" in the contraction whereas electrical- and perfusion-stimulated contractions appear to recover fully after a single stimulus. Additionally, laser activation stimulates cells 10 to 20 cells distant from the activation site whereas nano-perfusion stimulates contraction only within cells that contact the lysate. These differences are relatively minor considering the diverse stimuli and the geometry of the epithelial tissues driven to contract. Lastly, we demonstrate that all three methods drive rapid remodeling of the F-actin cytoskeleton. Recent work suggests that mechanical stimuli may induce contractions in Drosophila embryonic epithelia [24,25], however mechanical stimulation was not sufficient to induce contractions here.

Each of the three methods to stimulate contraction has advantages in future studies. The micro-aspiration technique is the best suited for biophysical and biomechanical studies, providing mechanical properties such as viscoelasticity of embryonic tissues and high-resolution kinematics of tissue responses to electrical stimulation. Electrically- and biochemically-induced contractions have been observed previously in chick embryos ([26,27] and [28], respectively); however the combination of electrically induced contraction with micro-aspiration provides a novel tool for analyzing the mechanics of contractions.

We used this tool to test the hypothesis that the capacity to produce force is positively related to tissue stiffness. Previous studies have found that primary invagination during sea urchin gastrulation [22,29], and *Xenopus* blastopore closure [14] and dorsal elongation [23] occur successfully despite considerable variation in tissue stiffness. We proposed that coupling between tissue stiffness and cellular force production could explain these observations. Surprisingly, we find no evidence for coupling between force generation and stiffness in electrically stimulated micro-aspirated tissue. Little data exists on tissue stiffness in other embryos, and data on forces driving morphogenesis (e.g. in Drosophila [30]) are almost entirely relative magnitudes, rather than absolute magnitudes, making comparisons impossible.

Laser-mediated photochemical, photothermal, and photomechanical methods have been used to perturb or ablate live tissues [31–34]. In cell and development biology, lasers have been used to ablate specific targets to investigate questions such as the role of the nucleus in dorso-ventral patterning of the egg [35], the role of cell rearrangement in sea urchin gastrulation [36], and the role of actomyosin contractile ring in single cell wounds in *Xenopus laevis* oocytes [37,38]. Because of its advantages for visualization, laser-activation is best suited to investigating the cell and molecular pathways that mediate cell contraction and biophysical events that couple actomyosin contraction to cell shape change. In some respects, our studies on a complex multicellular epithelial sheet appear analogous to the wounding studies in the single-cell *Xenopus* oocytes [37–39]. With laser-stimulated contraction, we observe that neighboring cells contract and F-actin remodeling begins within a few seconds.

We found that laser-activation induces isometric contractility and global up-regulation of F-actin at large distances from the laser-activated site (at least 250 μm). Previous wounding studies have demonstrated very limited up-regulation of actomyosin in a ring around wounds within single cells [37], or immediately adjacent cells in a ring around the wound in epithelial sheets [8,40–42]. These studies have not reported contractile responses within wounded cells or their surrounding tissues. Our novel observations may be due to the freedom of embryonic tissues to deform. Cells cultured on glass or plastic or bound to rigid ECM scaffolds may not visibly deform. Based on previous studies of wounding responses [40] and spontaneous contractions [43] in *Xenopus* we suggest that laser activation may induce a calcium wave in the surrounding tissue that activates actin polymerization and myosin contractility through Rho and/or Cdc42 dependent pathways. Given the similar kinematics and F-actin dynamics exhibited by contractions induced by the three methods described here, we suggest that at least the downstream events of the pathway are shared among all three types of induced contraction.

Neither laser-activation nor electrical stimulation is a likely event within the embryo but perfusion induced stimulation may have a physiological role. Cell contraction in response to chemical stimuli is likely due to a pre-existing receptor that can “trigger” contraction within epithelial cells in the embryo. A number of possible such triggers have been identified in other systems [24,28]. While both laser-activation and lysate may trigger wound response pathways, the factor(s) within lysate may also have signaling roles during morphogenesis.

Both spontaneous and periodic contractions have been observed in *Xenopus* gastrula [43] as well as gastrulating chick embryos [26,44]. These rare spontaneous contractions exhibit similar kinematics to the contractions we induce in this paper. Such contractions may be more common than reported since they form and dissipate faster than the 2 to 5 minute time-lapse intervals typically used to study morphogenetic movements. Periodic contractions in epithelial cells precede epithelial morphogenetic movements in Drosophila and suggest that embryonic tissues are a form of “excitable media” [8,24,25]. We speculate that pathways controlling acute contraction could trigger excitable tissues or coordinate cell contraction during large scale movements such as neurulation. Testing candidate pathways revealed in *Drosophila* genetic

studies and the identification of the factor(s) within cell lysate will be key prerequisites to future progress.

Supplementary Material

Refer to Web version on PubMed Central for supplementary material.

Acknowledgments

This work was supported by a grant to LD from the National Institutes of Health (R01-HD044750) and support from the American Heart Association (Beginning Grant-in-Aid). The authors thank Lin Zhang (Davidson lab) and Larry Phillips for their assistance. We thank Photonic Instruments Inc. (Saint Charles, IL) for the gracious loan of the Micropoint System. We thank Dr. Doug Weber, Dr. Tracy Cui, Joost Wagenaar, and Jim Hokanson for their guidance in developing electrical stimulation protocols and William Bement and John Wallingford for their kind gifts of plasmids encoding F-actin reporters utrophin-GFP and moesin-GFP, respectively.

References

1. Nakajima Y, Burke RD. The initial phase of gastrulation in sea urchins is accompanied by the formation of bottle cells. Dev Biol 1996;179:436–446. [PubMed: 8903358]
2. Leptin M, Grunewald B. Cell shape changes during gastrulation in Drosophila. Development 1990;110 (1):73–84. [PubMed: 2081472]
3. Smith JL, Schoenwolf GC. Neurulation: coming to closure. Trends Neurosci 1997;20:510–517. [PubMed: 9364665]
4. Smith JL, Schoenwolf GC, Quan J. Quantitative analyses of neuroepithelial cell shapes during bending of the mouse neural plate. J Comp Neurol 1994;342:144–151. [PubMed: 8207124]
5. Shook D, Keller R. Mechanisms, mechanics and function of epithelial-mesenchymal transitions in early development. Mech Dev 2003;120:1351–1383. [PubMed: 14623443]
6. Toyama Y, Peralta XG, Wells AR, Kiehart DP, Edwards GS. Apoptotic force and tissue dynamics during Drosophila embryogenesis. Science 2008;321:1683–1686. [PubMed: 18802000]
7. Davidson LA, Ezin AM, Keller R. Embryonic wound healing by apical contraction and ingression in *Xenopus* laevis. Cell Motil Cytoskeleton 2002;53:163–176. [PubMed: 12211099]
8. Martin AC, Kaschube M, Wieschaus EF. Pulsed contractions of an actin-myosin network drive apical constriction. Nature 2009;457:495–499. [PubMed: 19029882]
9. Young PE, Pesacreta TC, Kiehart DP. Dynamic changes in the distribution of cytoplasmic myosin during Drosophila embryogenesis. Development 1991;111(1):1–14. [PubMed: 1901784]
10. Davidson LA, Von Dassow M, Zhou J. Multi-scale mechanics from molecules to morphogenesis. International Journal of Biochemistry and Cell Biology. 2009
11. Kay, BK.; Peng, HB. Xenopus laevis: practical uses in cell and molecular biology. Academic Press; New York: 1991.
12. Nieuwkoop, PD.; Faber, J. Normal tables of Xenopus laevis (Daudin). Elsevier North-Holland Biomedical Press; Amsterdam: 1967.
13. Sater AK, Steinhardt RA, Keller R. Induction of neuronal differentiation by planar signals in *Xenopus* embryos. Dev Dyn 1993;197:268–280. [PubMed: 8292824]
14. von Dassow M, Davidson LA. Natural variation in embryo mechanics: gastrulation in *Xenopus laevis* is highly robust to variation in tissue stiffness. Dev Dyn 2009;238:2–18. [PubMed: 19097119]
15. Aoki T, Ohashi T, Matsumoto T, Sato M. The pipette aspiration applied to the local stiffness measurement of soft tissues. Ann Biomed Eng 1997;25:581–587. [PubMed: 9146811]
16. Boudou T, Ohayon J, Arntz Y, Finet G, Picart C, Tracqui P. An extended modeling of the micropipette aspiration experiment for the characterization of the Young's modulus and Poisson's ratio of adherent thin biological samples: numerical and experimental studies. J Biomech 2006;39:1677–1685. [PubMed: 15978599]
17. Lee JY, Harland RM. Actomyosin contractility and microtubules drive apical constriction in *Xenopus* bottle cells. Dev Biol 2007;311:40–52. [PubMed: 17868669]

18. Litman P, Amieva MR, Furthmayr H. Imaging of dynamic changes of the actin cytoskeleton in microextensions of live NIH3T3 cells with a GFP fusion of the F-actin binding domain of moesin. BMC Cell Biol 2000;1:1. [PubMed: 11112983]
19. Burkel BM, von Dassow G, Bement WM. Versatile fluorescent probes for actin filaments based on the actin-binding domain of utrophin. Cell Motil Cytoskeleton 2007;64:822–832. [PubMed: 17685442]
20. Schafer DA, Welch MD, Machesky LM, Bridgman PC, Meyer SM, Cooper JA. Visualization and molecular analysis of actin assembly in living cells. J Cell Biol 1998;143:1919–1930. [PubMed: 9864364]
21. Orth JD, Krueger EW, Cao H, McNiven MA. The large GTPase dynamin regulates actin comet formation and movement in living cells. Proc Natl Acad Sci U S A 2002;99:167–172. [PubMed: 11782546]
22. von Dassow M, Davidson LA. Variation and robustness of the mechanics of gastrulation: the role of tissue mechanical properties during morphogenesis. Birth Defects Res C Embryo Today 2007;81:253–269. [PubMed: 18228257]
23. Zhou J, Kim HY, Davidson LA. Actomyosin stiffens the vertebrate embryo during critical stages of elongation and neural tube closure. Development 2009;136:677–688. [PubMed: 19168681]
24. Pouille PA, Ahmadi P, Brunet AC, Farge E. Mechanical signals trigger Myosin II redistribution and mesoderm invagination in Drosophila embryos. Sci Signal 2009;2:ra16. [PubMed: 19366994]
25. Solon J, Kaya-Copur A, Colombelli J, Brunner D. Pulsed forces timed by a ratchet-like mechanism drive directed tissue movement during dorsal closure. Cell 2009;137:1331–1342. [PubMed: 19563762]
26. Kucera P, Burnand MB. Mechanical tension and movement in the chick blastoderm as studied by real-time image analysis. J Exp Zool Suppl 1987;1:329–339. [PubMed: 3598500]
27. Kucera P, de Ribaupierre Y. In situ recording of the mechanical behaviour of cells in the chick embryo. Prog Clin Biol Res 1982;85 Pt B:433–444. [PubMed: 7122575]
28. Drews U, Mengis W. Contraction wave in the chick blastoderm induced by muscarinic stimulation. Anat Embryol (Berl) 1990;182:447–454. [PubMed: 2291489]
29. Davidson LA, Oster GF, Keller RE, Koehl MA. Measurements of mechanical properties of the blastula wall reveal which hypothesized mechanisms of primary invagination are physically plausible in the sea urchin Strongylocentrotus purpuratus. Dev Biol 1999;209:221–238. [PubMed: 10328917]
30. Hutson MS, Tokutake Y, Chang MS, Bloor JW, Venakides S, Kiehart DP, Edwards GS. Forces for morphogenesis investigated with laser microsurgery and quantitative modeling. Science 2003;300:145–149. [PubMed: 12574496]
31. Rau KR, Quinto-Su PA, Hellman AN, Venugopalan V. Pulsed laser microbeam-induced cell lysis: time-resolved imaging and analysis of hydrodynamic effects. Biophys J 2006;91:317–329. [PubMed: 16617076]
32. Venugopalan V, Guerra A 3rd, Nahen K, Vogel A. Role of laser-induced plasma formation in pulsed cellular microsurgery and micromanipulation. Phys Rev Lett 2002;88:078103. [PubMed: 11863944]
33. Vogel A, Venugopalan V. Mechanisms of pulsed laser ablation of biological tissues. Chem Rev 2003;103:577–644. [PubMed: 12580643]
34. Vogel A, Linz N, Freidank S, Paltauf G. Femtosecond-laser-induced nanocavitation in water: implications for optical breakdown threshold and cell surgery. Phys Rev Lett 2008;100:038102. [PubMed: 18233040]
35. Montell DJ, Keshishian H, Spradling AC. Laser ablation studies of the role of the Drosophila oocyte nucleus in pattern formation. Science 1991;254:290–293. [PubMed: 1925585]
36. Hardin J. The role of secondary mesenchyme cells during sea urchin gastrulation studied by laser ablation. Development 1988;103(2):317–324. [PubMed: 3224556]
37. Benink HA, Bement WM. Concentric zones of active RhoA and Cdc42 around single cell wounds. J Cell Biol 2005;168:429–439. [PubMed: 15684032]
38. Mandato CA, Bement WM. Contraction and polymerization cooperate to assemble and close actomyosin rings around *Xenopus* oocyte wounds. J Cell Biol 2001;154:785–797. [PubMed: 11502762]

39. Mandato CA, Bement WM. Actomyosin transports microtubules and microtubules control actomyosin recruitment during *Xenopus* oocyte wound healing. Curr Biol 2003;13:1096–1105. [PubMed: 12842008]

40. Clark AG, Miller AL, Vaughan E, Yu HY, Penkert R, Bement WM. Integration of Single and Multicellular Wound Responses. Curr Biol. 2009

41. Fenteany G, Janmey PA, Stossel TP. Signaling pathways and cell mechanics involved in wound closure by epithelial cell sheets. Curr Biol 2000;10:831–838. [PubMed: 10899000]

42. Wood W, Jacinto A, Grose R, Woolner S, Gale J, Wilson C, Martin P. Wound healing recapitulates morphogenesis in Drosophila embryos. Nat Cell Biol 2002;4:907–912. [PubMed: 12402048]

43. Wallingford JB, Ewald AJ, Harland RM, Fraser SE. Calcium signaling during convergent extension in *Xenopus*. Curr Biol 2001;11:652–661. [PubMed: 11369228]

44. Stern CD, Goodwin BC. Waves and periodic events during primitive streak formation in the chick. Journal of Embryology and Experimental Morphology 1977;41:15–22. [PubMed: 591867]

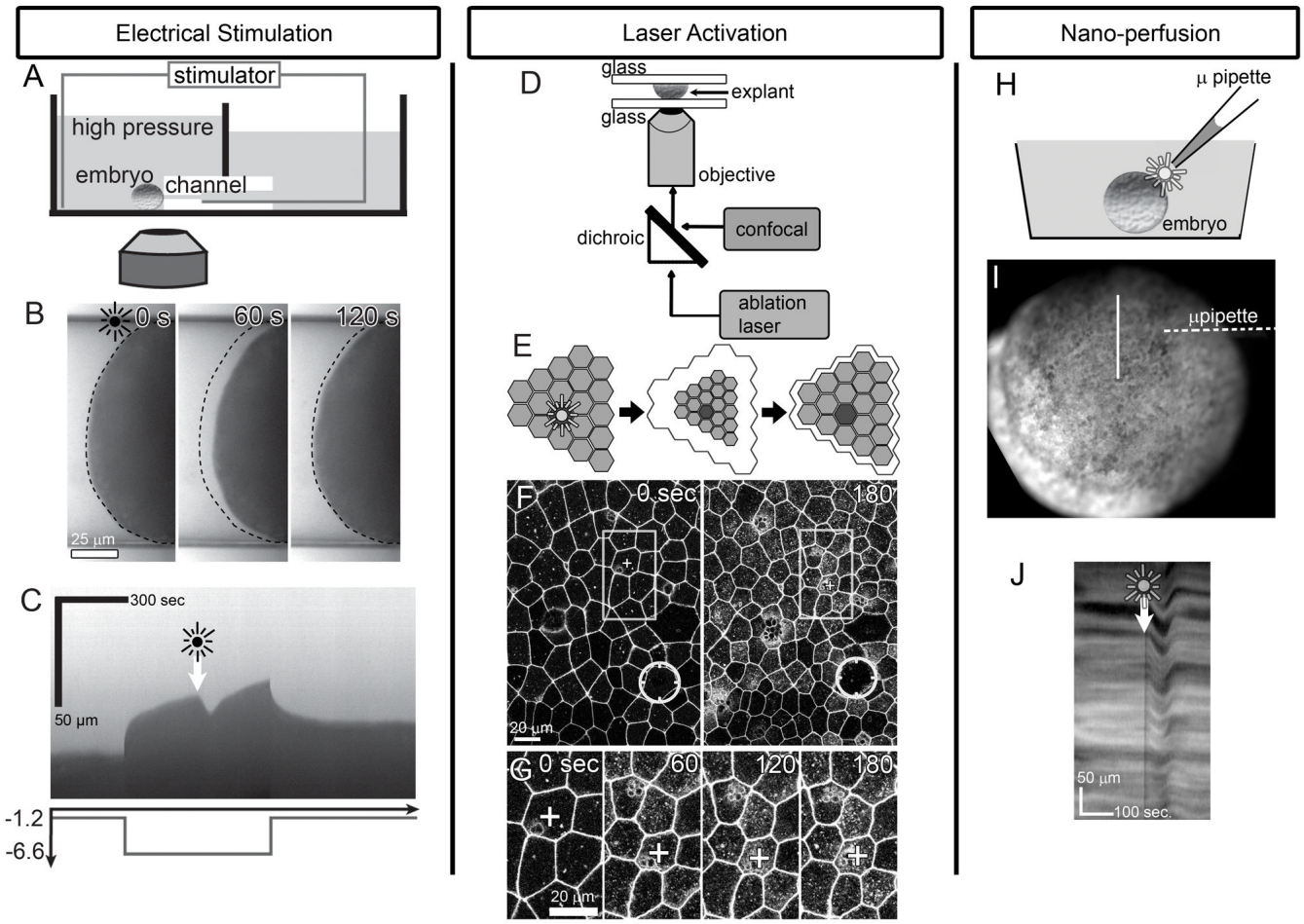

Figure 1. Stimulated cell contraction via electrical pulse, laser-activation, and nano-perfusion

A) Stimulation of an embryo held within a micro-aspirator. B) Aspirated tissues show time-course of stimulated contraction and post-stimulation relaxation. (dotted line, limit of aspiration prior to the stimulus; see supplemental video S1). C) Kymograph along middle of the micro-channel illustrates the viscoelastic response to drop in pressure (Pa) over time (graph shown below kymograph) and response to stimulus (arrow and starburst). D) Schematic of laser-activation of animal cap explant. E) Activation or ablation of a single cell (starburst) results in contraction of a large field of epithelial cells. F) Time-lapse sequences collected over a large field of cells shows contractions spread at least 10 cell-diameters away from the ablation site (circle; see supplemental video S2). G) High resolution view of cells 2- to 6-cell diameters from stimulus (boxes in panel F) contract over 3 minutes. ("+" cell is the same in F and G) H) Schematic of nano-perfusion shows delivery of 60 nl of cell lysate (starburst) to an embryo (I). J) Time-lapse sequences of the surface of the embryo (in I) resolves the contractile response in a kymograph (along line in I; see supplemental video S3).

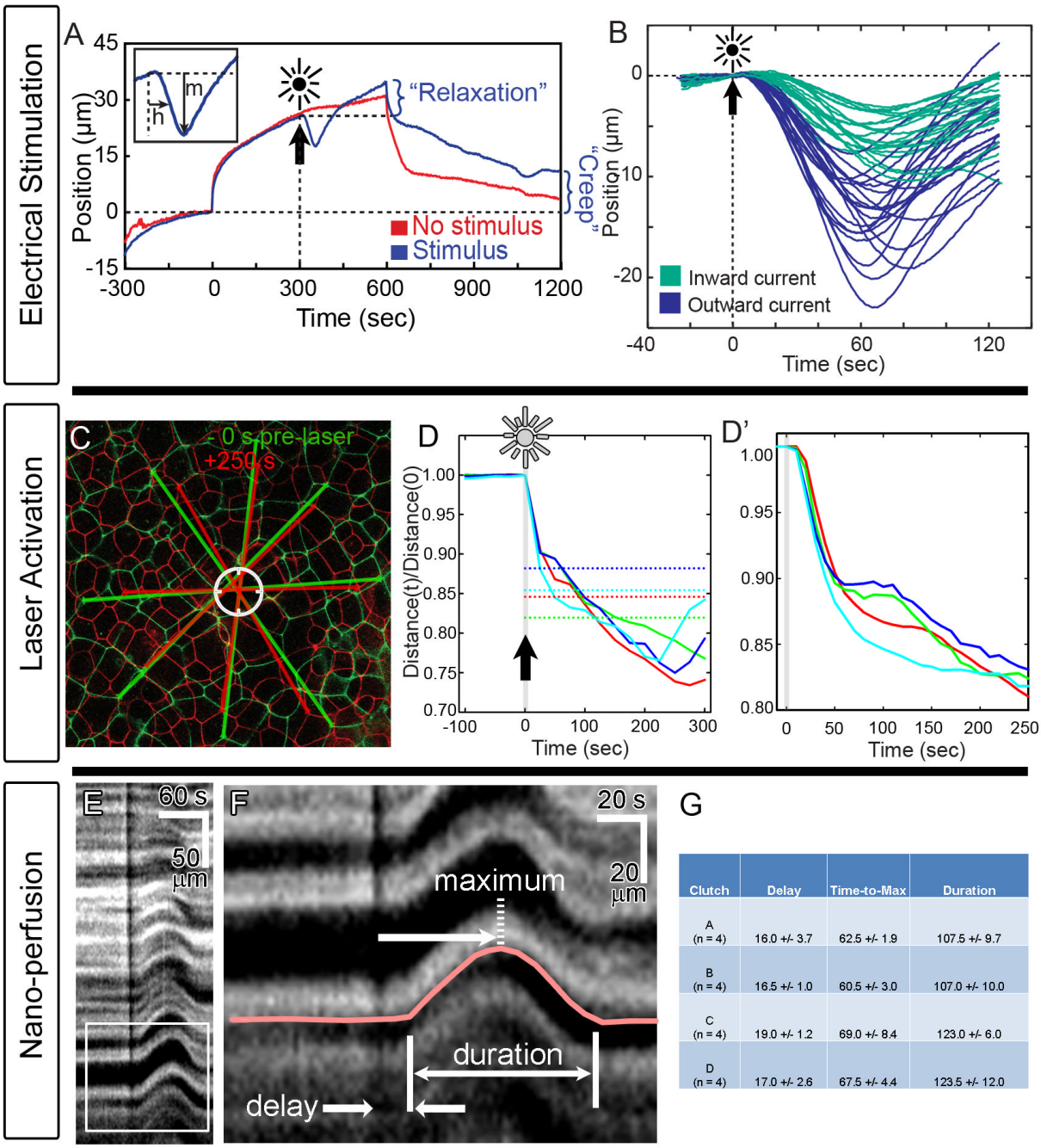

Clutch	Delay	Time-to-Max	Duration
A (n = 4)	16.0 +/- 3.7	62.5 +/- 1.9	107.5 +/- 9.7
B (n = 4)	16.5 +/- 1.0	60.5 +/- 3.0	107.0 +/- 10.0
C (n = 4)	19.0 +/- 1.2	69.0 +/- 8.4	123.0 +/- 6.0
D (n = 4)	17.0 +/- 2.6	67.5 +/- 4.4	123.5 +/- 12.0

Figure 2. Kinematic responses to stimuli

A) Response to electrical stimulus is tracked by the distance it retracts down the micro-aspirator channel ("m"), and the time to half maximal retraction ("h"). Pressure drop from −1.2 Pa to −6.6 Pa occurs at 0 seconds and pressure restored after 600 seconds. B) Electrical stimulus consistently induces contraction but the magnitude of contraction varies with the polarity of the applied stimulus. Each line records a separate stimulation. C) Tissue contraction response to laser activation (circle) can be seen in an overlay of cell boundaries before and after stimulation. D) The time-course of 4 representative experiments show a 10 to 20 second delay followed by rapid contraction over 50 seconds (D′). Dotted lines indicate the contraction needed to remove or replace tissue damaged by laser in each experiment. E & F) The contraction

response to nano-perfusion as seen in kymographs (F: enlargement of box in E) reveals a 15 to 20 second delay followed by rapid contraction over 40 to 50 seconds (G). The black vertical line in E and F indicates perfusion of ink-labeled lysate.

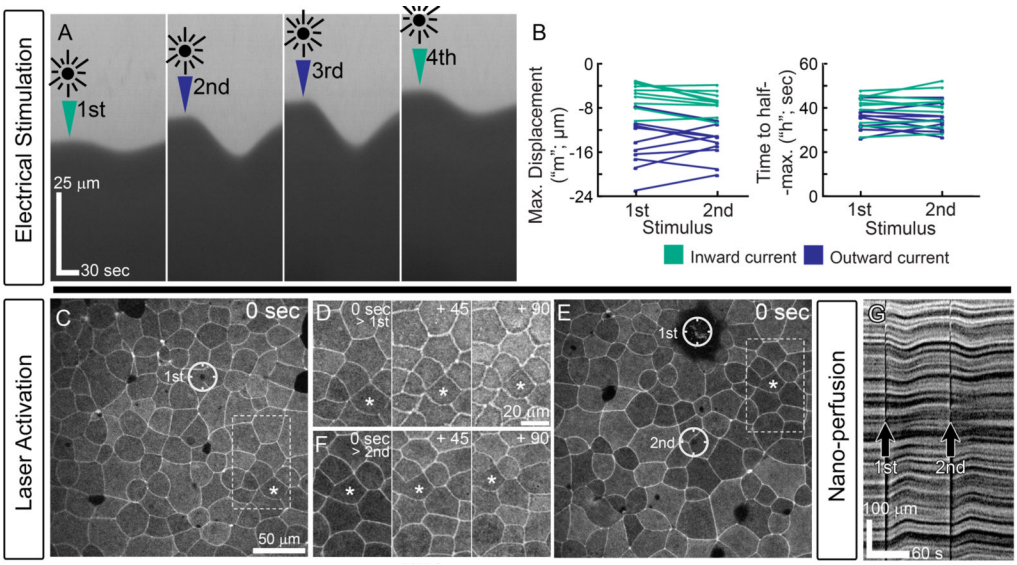

Figure 3. Embryonic epithelium is sensitive to repeated stimuli

A) Four electrical stimuli applied to micro-aspirated embryos show no difference in the response between the first and second stimulus in a given current direction (B). C) Multiple laser stimulations in the same field (single circle in C and two circles in E) induce similar responses in cells 2 to 6 cell diameters away (D for single stimulus and F following second stimulus; asterisked cell is the same in panels C through F). G) Multiple perfusion stimulations also produce multiple contractions.

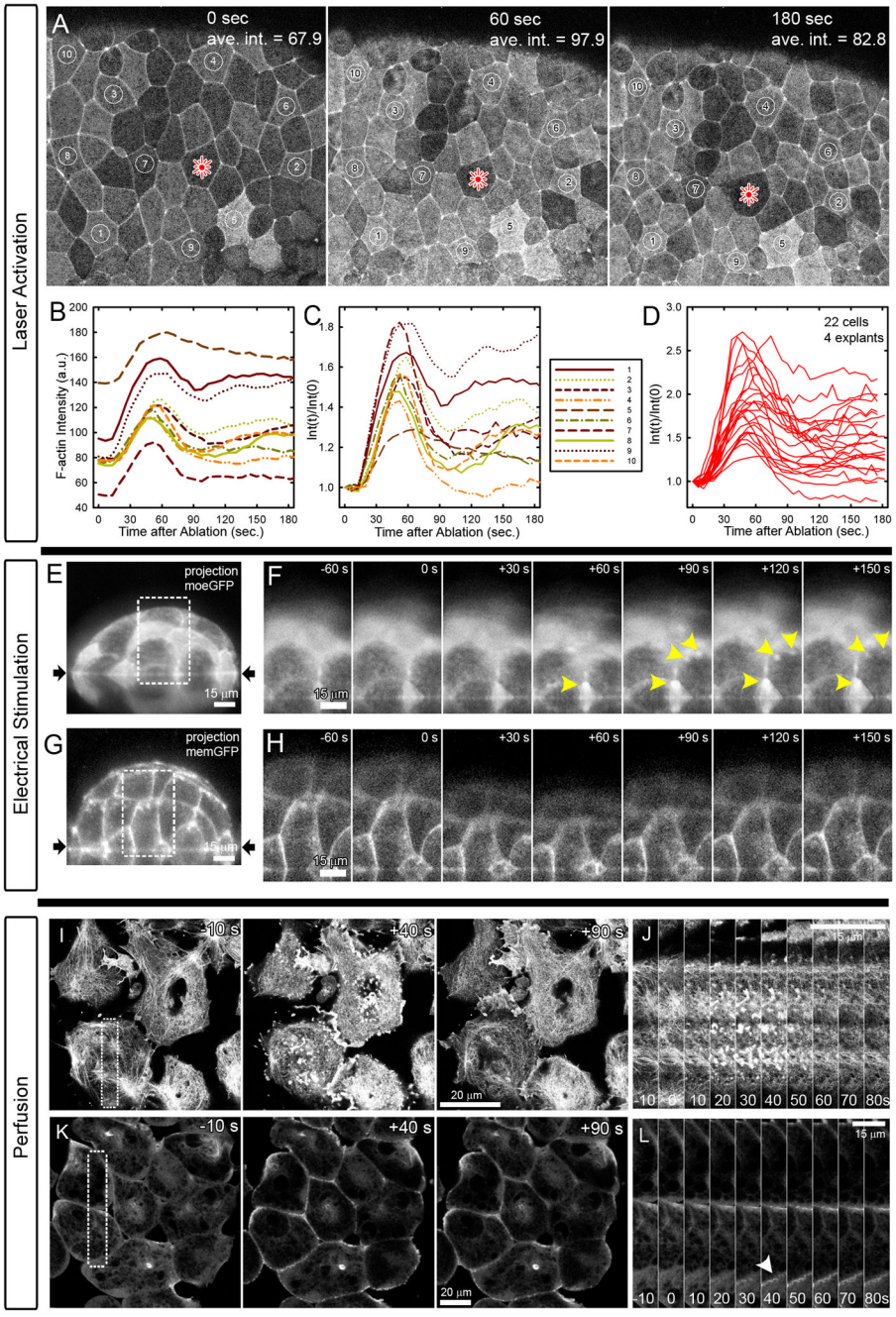

Figure 4. Stimulation induces F-actin remodeling

A) Laser-activation induces F-actin (actin-binding fragment of moesin-GFP) accumulation within surrounding epithelium (see Supplementary movie S5). B) Intensity of F-actin shows consistent rapid increase followed by variable reduction that does not depend on the initial intensity of the contracting cell (C). D) 22 cells from 4 explants show consistent initial increase followed by variable degrees of reduction. E) Side view of micro-aspirated tissue expressing moesin-GFP shows increasing F-actin (F) within transient actin 'comets' (yellow arrowheads; see Supplementary movie S6). G) Plasma membrane labeled tissues do not show increases (H). I) Response to perfusion of animal cap explants show rapid disassembly and transient formation of high intensity actin comets and foci within the basal cell cortex over 90 seconds (J). K) A

deeper confocal section, 5 μm from the basal surface shows F-actin within the lateral cell cortex (at cell-cell boundaries: arrowhead) also intensifies and remodels in response to perfusion of cell lysate (L).

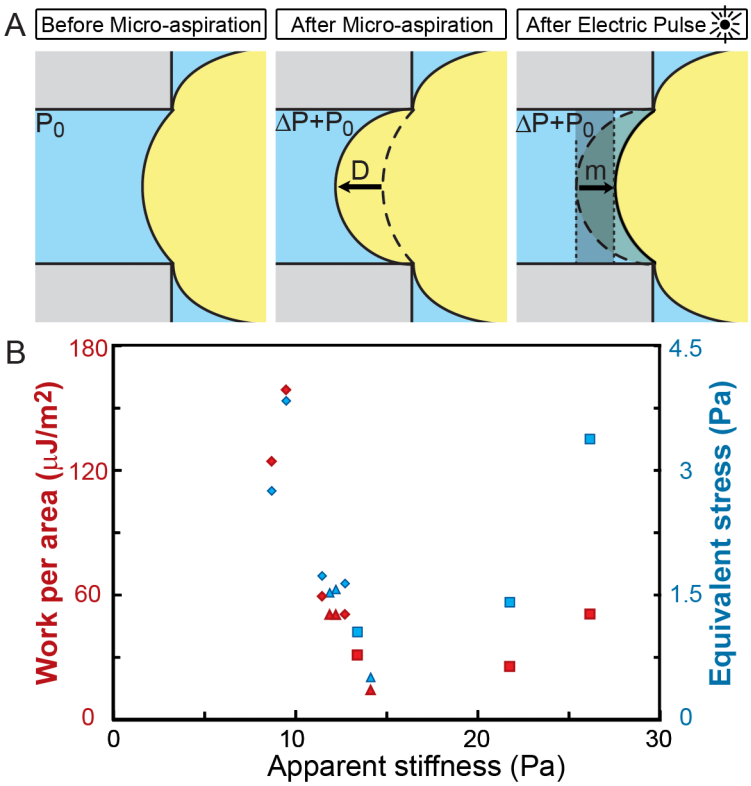

Figure 5. Mechanical force and work of contraction

A) Schematic showing progressive tissue shape changes during electrical stimulation (embryo not to scale relative to channel). Geometrical tissue shape changes from micro-aspiration allow estimation of apparent stiffness from the load pressure (ΔP) and the depth of aspiration into the micro-channel (D). Tissue shape changes after electrical stimulation allow estimation of the forces generated during contraction and the work of contraction as the tissue withdraws from the micro-channel (m) against the applied pressure. B) Red symbols indicate Work per area and blue indicate Equivalent stress. Each data point is from a single embryo and similar shapes are from the same clutch.

Table 1

ANOVAs for creep and relaxation following electrical stimulation: *P*-values (F-statistic).

Factor	Relaxation (μm)	Creep (μm)	Relaxation*	Creep*
Stimulus	0.9 ($F_{1,2}$ = 0.04)	0.6 ($F_{1,2}$ = 0.32)	0.7 ($F_{1,2}$ = 0.15)	0.6 ($F_{1,2}$ = 0.48)
Clutch	0.6 ($F_{2,2}$ = 0.56)	0.6 ($F_{2,2}$ = 0.71)	0.8 ($F_{2,2}$ = 0.23)	0.7 ($F_{2,2}$ = 0.38)
Clutch × Stimulus	0.003 ($F_{2,14}$ = 9.40)	0.015 ($F_{2,13}$ = 5.94)	0.006 ($F_{2,14}$ = 7.58)	0.005 ($F_{2,13}$ = 8.30)

* Normalized to displacement following suction (at 300 s).

n = 9 to 10 embryos per treatment from 3 clutches (3 to 4 embryos per clutch).

Table 2

ANOVAs for work and equivalent stress of electrically induced contractions: *P*-values (F-statistic).

Factor	Work ($\mu J/m^2$)	Equivalent stresss (Pa)
Stiffness*	0.06 ($F_{1,4}$ = 6.97)	0.2 ($F_{1,4}$ = 2.45)
Clutch	0.05 ($F_{2,4}$ = 7.32)	0.09 ($F_{2,4}$ = 4.74)
Clutch × Stiffness*	0.06 ($F_{2,4}$ = 6.50)	0.1 ($F_{2,4}$ = 4.04)

*Apparent stiffness (Pa) measured at 300 s after suction.

n = 10 embryos from 3 clutches (3 to 4 embryos per clutch).